

HOW COSMIC WEB ENVIRONMENT AFFECTS GALAXY QUENCHING ACROSS COSMIC TIME

FARHANUL HASAN ¹, JOSEPH N. BURCHETT ¹, ALYSSA ABEYTA,¹ DOUGLAS HELLINGER,² NIR MANDELKER ³,
JOEL R. PRIMACK ², SANDRA FABER ², DAVID C. KOO ⁴, OSKAR ELEK ⁵ AND DAISUKE NAGAI ⁶

¹Department of Astronomy, New Mexico State University, Las Cruces, NM 88003, USA

²Department of Physics, University of California, Santa Cruz, CA 95064, USA

³Centre for Astrophysics and Planetary Science, Racah Institute of Physics, The Hebrew University, Jerusalem 91904, Israel

⁴Department of Astronomy and Astrophysics, University of California, Santa Cruz, Santa Cruz, CA 95064, USA

⁵Department of Computational Media, University of California, 1156 High Street, Santa Cruz, CA 95064, USA

⁶Department of Physics, Yale University, New Haven, CT 06520, USA

ABSTRACT

We investigate how cosmic web structures affect galaxy quenching in the IllustrisTNG (TNG-100) cosmological simulations by reconstructing the cosmic web in each snapshot using the DISPERSE framework. We measure the distance from each galaxy with stellar mass $\log(M_*/M_\odot) \geq 8$ to the nearest node (d_{node}) and the nearest filament spine (d_{fil}) and study the dependence of both median specific star formation rate ($\langle \text{sSFR} \rangle$) and median gas fraction ($\langle f_{\text{gas}} \rangle$) on these distances. We find that $\langle \text{sSFR} \rangle$ of galaxies is only dependent on cosmic web environment at $z < 2$, with the dependence increasing with time. At $z \leq 0.5$, $8 \leq \log(M_*/M_\odot) < 9$ galaxies are quenched at $d_{\text{node}} \lesssim 1$ Mpc, and significantly star formation-suppressed at $d_{\text{fil}} \lesssim 1$ Mpc, trends which are driven mostly by satellite galaxies. At $z \leq 1$, in contrast to the monotonic rise in $\langle \text{sSFR} \rangle$ of $\log(M_*/M_\odot) < 10$ galaxies with d_{node} and d_{fil} , $\log(M_*/M_\odot) \geq 10$ galaxies actually experience an upturn in $\langle \text{sSFR} \rangle$ at $d_{\text{node}} \lesssim 0.2$ Mpc (this is caused by both satellites and centrals). Much of this cosmic web-dependence of star formation activity can be explained by the evolution in $\langle f_{\text{gas}} \rangle$. Our results suggest that in the past ~ 10 Gyr, low-mass satellites are quenched by rapid gas stripping in dense environments near nodes and gradual gas starvation in intermediate-density environments near filaments, while at earlier times cosmic web structures efficiently channeled cold gas into most galaxies. State-of-the-art ongoing spectroscopic surveys such as SDSS and DESI, as well as those planned with *JWST* and *Roman*, are required to test our predictions against observations.

Keywords: Cosmic web (330), Large-scale structure of the universe (902), Galaxy quenching (2040), Galaxy evolution (594), Intergalactic filaments (811), Magnetohydrodynamical simulations (1966)

1. INTRODUCTION

In the standard cosmological model, structure formation in the universe occurs at vastly different scales. Galaxies form stars within tens of kpc and grow inside dark matter (DM) halos which can be two orders of magnitude larger. At even larger scales, galaxies and their DM halos are embedded within an intricate network of strand-like filaments, diffuse sheets, dense nodes, and underdense voids, which is termed the “cosmic web” (e.g., Bond et al. 1996; Springel et al. 2005). While the cosmic web has been studied on both theoretical and observational grounds for decades, it remains one of the major outstanding questions in astrophysics how the large-scale cosmic web environment influences the formation and evolution of galaxies.

A chief concern in galaxy evolution is how star formation activity proceeds in galaxies and how it ceases, i.e., how quenching occurs. It has long been known that quenching depends on internal mechanisms characterized by the stellar mass M_* or halo mass M_{vir} (e.g., Brinchmann et al. 2004; Cattaneo et al. 2006; Williams et al. 2009; Peng et al. 2010;

Darvish et al. 2016), such that galaxy-scale processes including supernovae (SNe) and Active Galactic Nuclei (AGN) feedback can regulate and curtail star formation activity. A widely adopted theoretical viewpoint posits that galaxies in halos with mass $\log(M_{\text{vir}}/M_\odot) \gtrsim 11.5 - 12$ can form stable virial accretion shocks and, therefore, a hot, hydrodynamically stable circumgalactic medium (CGM) that suppresses accretion of cold gas to the interstellar medium (ISM) necessary for star formation (e.g., Birnboim & Dekel 2003; Dekel & Birnboim 2006; Kereš et al. 2005, 2009; Dekel et al. 2009). Lower-mass galaxies (typically with $\log(M_*/M_\odot) < 10$) especially at high redshifts ($z \gtrsim 2$) lack this ability to form a stable hot CGM and “self-quench” (e.g., Croton et al. 2006; Gabor & Davé 2012).

External processes as characterized by their environment have also emerged as crucial factors in determining how galaxies quench (e.g., Elbaz et al. 2007; Peng et al. 2012; Eardley et al. 2015; Moutard et al. 2018; Bluck et al. 2020). However, the exact nature of the relationship between quenching and environment, and what physical mech-

anisms manifest this relationship, is a topic of widespread debate. In the hot, dense halos of galaxy groups and clusters, hydrodynamical interactions between the halo medium and satellite galaxies – most notably ram pressure stripping (e.g., Bahé & McCarthy 2015; Boselli et al. 2022) – or tidal interactions between separate galaxies or between galaxies and the halo (e.g., Boselli & Gavazzi 2006; Marasco et al. 2016) can remove the star-forming ISM of a galaxy. Over longer timescales, gas accretion on to the ISM can be halted, either due to lack of accretion from the intergalactic medium (IGM) to the CGM or from the CGM to the ISM, via strangulation or starvation (e.g., Larson et al. 1980; Balogh & Morris 2000; Peng et al. 2015).

The cosmic web itself has also been invoked in models of galaxy quenching. Aragon Calvo et al. (2019) proposed that “cosmic web detachment,” wherein galaxies are detached from cold gas-supplying primordial filaments, can explain much of the observed quenching phenomena across time. Song et al. (2021) suggested that galaxies that live close to the centers of filaments cannot transfer gas efficiently from the outer parts of halos to galactic centers due to lower angular momentum supply in these regions. Pasha et al. (2022) found that cosmological accretion shocks at $z \sim 2 - 5$ can produce a hot ($T > 10^6$ K) IGM at the edge of sheets, which can quench low-mass centrals at these epochs, as shocks around filaments, groups, and clusters can at lower redshifts (e.g., Birnboim et al. 2016; Zinger et al. 2018; Li et al. 2023).

Studies of the connection between galaxy quenching and the cosmic web in the past decade have yielded mixed results. While many observational studies have found that passive or quenched galaxies are typically located near nodes and filaments (e.g., Kuutma et al. 2017; Kraljic et al. 2018; Laigle et al. 2018; Winkel et al. 2021), some have shown that proximity to the cosmic web can also enhance star formation in galaxies (e.g., Darvish et al. 2014; Vulcani et al. 2019). Cosmological hydrodynamical simulations have also provided an inconclusive picture. In the IllustrisTNG simulations (Pillepich et al. 2018), Malavasi et al. (2022) found that the specific star formation rate ($\text{sSFR} = \text{SFR}/M_*$) of galaxies is generally reduced with proximity to nodes and filaments at $z = 0$. Xu et al. (2020) found in the EAGLE simulations (Schaye et al. 2015), a characteristic stellar mass ($\log(M_*/M_\odot) \sim 10.5$) below which galaxies have lower sSFR in nodes than in filaments and above which this dependence vanishes. Both Kotecha et al. (2022) and Zheng et al. (2022) reported evidence, instead, of filaments increasing star formation activity or at least delaying quenching. Singh et al. (2020) proposed accretion of intra-filamentary gas onto galaxies as a significant pathway to fueling star formation. Therefore, consensus is yet to be reached on the impact of cosmic web environment on galaxy quenching, and how this varies with stellar mass and redshift.

In this paper, we employ the IllustrisTNG cosmological simulations to study the impacts of cosmic web environment, particularly the proximity to filaments and nodes, on star formation and gas content in galaxies across cosmic time. We reconstruct the cosmic web in IllustrisTNG using

the topologically-motivated DISPERSE framework (Sousbie 2011; Sousbie et al. 2011). This is the first study of the dependence of star formation quenching on the cosmic web in the TNG100-1 run across many different redshift snapshots. Malavasi et al. (2022) performed a similar analysis of the TNG300-1 run at $z = 0$.

This paper is organized as follows. In Section 2, we describe the simulation data used in this work and methods of reconstructing the cosmic web. We present our results in Section 3. We discuss the physical interpretations of our results and propose observational tests in Section 4, and conclude in Section 5. We adopt the *Planck 2015* cosmology (Planck Collaboration et al. 2016), with $H_0 = 67.74 \text{ km s}^{-1} \text{ Mpc}^{-1}$, $\Omega_{\text{M},0} = 0.3089$, and $\Omega_{\Lambda,0} = 0.6911$. All distances are quoted in comoving units, unless stated otherwise.

2. DATA AND METHODS

2.1. TNG Simulations

We analyzed outputs from the IllustrisTNG-100 magnetohydrodynamic cosmological simulations (Pillepich et al. 2018; Nelson et al. 2019a), which uses the AREPO moving-mesh hydrodynamics code (Springel 2010) to simulate the evolution of gas, stars, DM, black holes (BH), and galaxies from the early universe ($z = 127$) to the present day ($z = 0$). In particular, we make use of TNG100-1, the highest resolution run of the TNG-100 simulations, which has a box size of ~ 110.7 comoving Mpc per side, minimum baryonic and DM particle mass of $\sim 1.4 \times 10^6 M_\odot$ and $\sim 7.5 \times 10^6 M_\odot$ respectively, a *Planck 2015* cosmology (Planck Collaboration et al. 2016), and 1820^3 initial DM particles. While TNG300-1 provides greater statistics of galaxies and cosmic structures with ≈ 20 times the volume of TNG100-1, it has $\approx 1/8$ the particle mass resolution. On the other hand, TNG50-1 provides $\approx 16\times$ greater particle mass resolution than TNG100-1, but has $\approx 1/10$ the volume.

We obtain galaxy data for all 100 snapshots of the TNG100-1 simulation (hereafter TNG) from the online data repository¹ (Nelson et al. 2019b). In each snapshot, “Group” catalogs are constructed using the friends-of-friends (FoF) substructure identification algorithm while the SUBFIND algorithm and searches for gravitationally bound objects in each FoF group representing either subhalos or the main (host) halo (Springel et al. 2001; Dolag et al. 2009). We make use of both the group and subhalo catalogs to identify halos and galaxies, respectively.

For each snapshot, we set a minimum stellar mass of $\log(M_*/M_\odot) = 8$, which corresponds to the typical minimum observable stellar mass of galaxies in the (nearby) universe and also ensures that the galaxies are well-resolved with at least about 100 stellar particles in them. Similarly, we set a minimum halo mass – corresponding to the mass enclosed in a sphere whose mean density is 200 times the critical density of the Universe – of $\log(M_{200,c}/M_\odot) = 9$ to ensure that each of the galaxies in our catalog reside inside halos that are well-resolved with at least 100 DM parti-

¹ <https://www.tng-project.org/data/>

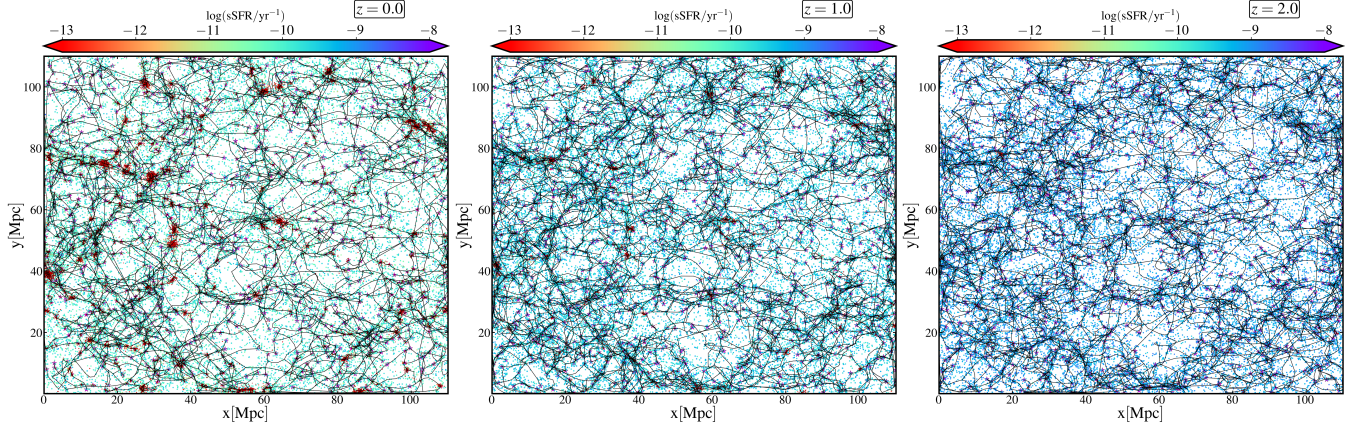


Figure 1. 2D visual representation of galaxies in the TNG-100 simulation and cosmic web structures identified by DISPERSE at $z = 0$ (left), $z = 1$ (middle), and $z = 2$ (right). In each panel, filament spines are represented by black curves, and nodes are represented by magenta stars, while galaxies are represented by scatter points sized by the stellar mass and color-coded by specific star formation rate. The same x-y projection is shown for each redshift. Quiescent galaxies at lower redshifts appear to be clustered closer to nodes and filaments.

cles. These criteria yielded $\sim 50,000$ galaxies at $z = 0$ and $\sim 11,000$ galaxies at $z = 5$. From these catalogs, we obtained galaxy comoving position, star formation rate (SFR), stellar mass (M_*), halo mass ($M_{200,c}$), halo virial radius ($R_{200,c}$; comoving radius at which $M_{200,c}$ is calculated), and mass of all gas gravitationally bound to a galaxy (M_{gas}). Hereafter, we refer to subhalos as galaxies and groups as halos.

2.2. Reconstructing the Cosmic Web with DISPERSE

Next, we apply the Discrete Persistent Structures Extractor (DISPERSE) algorithm (Sousbie 2011; Sousbie et al. 2011) to find cosmic web filaments and nodes in each TNG snapshot where at least 10,000 galaxies matched our selection criteria above. DISPERSE identifies the topology of space in any given volume based on an input distribution of discrete tracers, which in our case are the spatial locations of all galaxies matching our selection criteria above. To do this, it computes the density field from the inputs, using the Delaunay Tessellation Field Estimator (DTFE; Schaap & van de Weygaert 2000), wherein the entire volume is divided into tetrahedrons, with the positions of individual galaxies as vertices. During the tessellation, the density field at the position of each vertex of the tessellation is smoothed by averaging it with its two nearest neighbors. This is done in order to minimize contamination by shot noise and the detection of small-scale spurious features (see, e.g., Malavasi et al. 2022). DISPERSE calculates the gradient of the density field and identifies critical points where the gradient is zero. These correspond to the voids (minima), saddle points, and nodes (maxima) of the density field. Filaments consist of a series of segments connecting maxima to other critical points.

For each topologically significant pair of critical points, DISPERSE computes the persistence, which is defined as the ratio of the density value at the two critical points. Persistence is a simple measure of how robust topological structures, i.e., the identified critical points and filament segments, are to local variations, in this case of the density field measured from input galaxy positions. This sets the effective

significance level of the detected filaments and allows us to quantify the effect of shot noise in the input data. For our fiducial run, we choose a persistence threshold of 3σ , which has been known to eliminate most spurious filamentary features in the TNG simulations (e.g., Galárraga-Espinosa et al. 2020). By experimenting with cuts of 4σ and 5σ , we find that these miss fainter structures but nonetheless do not significantly alter our results.

In addition, we choose to apply a smoothing to the position of the segments of the filamentary skeleton by averaging the positions of the extrema of a segment with those of the extrema of contiguous segments. In essence, the skeleton is smoothed by keeping the critical points fixed and averaging the coordinates of each point along a filament with that of its two neighbors. This is done to reduce unphysical shapes of filament segments caused by shot noise, so that a smoother filamentary skeleton could be obtained. We find that increasing the amount of smoothing by one or removing this smoothing does not have a significant effect on our statistical results.

Furthermore, we experimented with varying the minimum stellar mass cut of our galaxy catalog and cosmic web reconstruction, using cuts of $\log(M_*/M_\odot) \geq 9$ and $\log(M_*/M_\odot) \geq 10$. These are more realistic minimum masses to compare to large, complete observational catalogs such as Sloan Digital Sky Survey (SDSS; e.g., Strauss et al. 2002) DR17 (see, e.g., Wilde et al. (2023), and Section 4.3 of this paper). However, the sharp drop in the number of galaxies in TNG with these higher masses yielded increasingly fewer input tracers for DISPERSE, which resulted in far fewer identified filaments and nodes than in our fiducial $\log(M_*/M_\odot) \geq 8$ cut, and particularly very few short filaments (with length $\lesssim 1$ Mpc). These higher mass cuts could therefore bias our results towards more prominent cosmic web features and longer filaments. In practice, varying the minimum $M_{200,c}$ cut was mostly degenerate with varying the minimum M_* cut.

A 2D visual representation of the DISPERSE-identified fil-

aments and nodes superimposed on the distribution of galaxies in TNG is shown in Fig. 1. The three panels show the $x - y$ projections across the whole volume at redshift $z = 0$ (left), $z = 1$ (middle), and $z = 2$ (right). In each panel, the filament spines and nodes are represented by black curves and magenta stars, respectively, while galaxies are represented by scatter points, with sizes proportional to M_* and color-coding by sSFR.

From this visualization, we can qualitatively assess the spatial distribution of star formation activity in galaxies with respect to cosmic web nodes and filaments. At any redshift, higher sSFR galaxies are located throughout the volume, whereas lower sSFR galaxies are almost always located close to a filament spine or a node. From higher to lower redshift (right to left panel), there is a clear decline in global star formation activity which is a representation of the decline in cosmic star formation activity after the so-called “cosmic noon” thoroughly chronicled in observations (e.g., [Madau & Dickinson 2014](#)). The number of massive quiescent galaxies increases considerably from $z = 2$ to $z = 1$ and even more prominently from $z = 1$ to the present day. A rough qualitative check showed us that virtually all $\text{SFR} = 0$ galaxies at low redshift, regardless of mass, live near nodes and/or filaments (we quantify a galaxy’s proximity to these cosmic web structures below).

2.3. Defining Distances

To quantitatively study the relationship between the physical properties of a galaxy and its cosmic web environment, we measure two different distances for each galaxy at each snapshot: d_{node} – the comoving Euclidean distance from the center of a galaxy to the center of the nearest identified node, and d_{fil} – the comoving transverse distance from the center of a galaxy to the nearest identified filament spine. These cosmic web-centric distance characterizations are similar to those of [Welker et al. \(2020\)](#) and [Malavasi et al. \(2022\)](#), among others. In the following, we investigate how star formation quenching and gas reservoirs of TNG galaxies is dependent on d_{node} and d_{fil} at different masses and redshifts.

3. RESULTS

3.1. Star Formation And Cosmic Web Environment

We first investigate the relationship between star formation activity of galaxies and their proximity to cosmic web structures. In each snapshot, we divide galaxies in three different stellar mass ranges – $8 \leq \log(M_*/M_\odot) < 9$, $9 \leq \log(M_*/M_\odot) < 10$, and $\log(M_*/M_\odot) \geq 10$ – into seven bins of the distances d_{node} and d_{fil} . These bins are chosen such that they have an equal number of galaxies inside of them. We measure the median sSFR, $\langle \text{sSFR} \rangle$, for each bin of d_{node} and d_{fil} . Experimenting with different numbers of bins, we find the overall results to be insensitive to the number of bins.

The results of these binned statistics are presented in Fig. 2, the top row showing $\langle \text{sSFR} \rangle$ as a function of d_{node} and the bottom row $\langle \text{sSFR} \rangle$ as a function of d_{fil} , and each column represent a different mass range. The $\langle \text{sSFR} \rangle$ in different bins of d_{node} or d_{fil} for a given redshift are plotted as dif-

ferent colored points and associated error bars; vertical error bars represent $\pm 1\sigma$ bootstrapped errors on $\langle \text{sSFR} \rangle$ in that bin, and horizontal error bars represent the width of the bin. Dotted curves represent simple spline interpolation fits to the $\langle \text{sSFR} \rangle$ - d_{node} and $\langle \text{sSFR} \rangle$ - d_{fil} relations. For a finer look at some intermediate redshifts, each panel also contains an inset showing a color contour plot for each snapshot between $z = 0.5$ and $z = 3$. For certain bins, we show an upper limit on $\langle \text{sSFR} \rangle$, corresponding to $\text{SFR} = 10^{-2.5} M_\odot \text{ yr}^{-1}$ which is the minimum resolvable SFR (averaged over 200 Myr) in TNG due to stochastic star formation with a minimum star particle mass (see [Terrazas et al. 2020](#)). For example, for $8 \leq \log(M_*/M_\odot) < 9$ galaxies, the maximum upper limit in sSFR is $10^{-11.5} \text{ yr}^{-1}$, considering the most massive galaxies in this mass range.

In order to separate the effect of nearby nodes from that of filaments alone (since many galaxies that are close to filament spines are also close to nodes), we only considered galaxies which are $d_{\text{node}} > 1$ Mpc away from the nearest node for the bottom row of Fig. 2. The choice of 1 Mpc is motivated by two considerations. 1) This is slightly higher than the virial radius $R_{200,c}$ of the most massive galaxy cluster in TNG-100. Therefore, this ensures that we remove possible halo-centric effects of nearby clusters and groups (which reside in nodes) and essentially only consider the effect of nearby filaments. 2) This is four times the scale radius of the filament galaxy density profile derived for TNG-300 filaments by [Galárraga-Espinosa et al. \(2020\)](#) and corresponds to the width containing almost all of the matter inside of filaments. We vary this cut to be $d_{\text{node}} > 0.5, 1.5$, and 2 Mpc as well and find that only galaxies at $z \lesssim 1$ with $d_{\text{fil}} < 1$ Mpc show noticeable changes to our quantitative results, while the qualitative results described below remain unchanged. In essence, this d_{node} cut ensures that only galaxies at intermediate to high, rather than extremely high, local densities are considered for the d_{fil} analysis (see [Burchett et al. 2020](#), for an example of how cosmic matter densities relate to different filamentary environments).

First, examining the node-centric relationships, we find that d_{node} is strongly correlated with quenching of star formation in lower mass galaxies ($\log(M_*/M_\odot) < 10$) at low redshifts ($z \lesssim 0.5$). For $8 \leq \log(M_*/M_\odot) < 9$ galaxies at $z \leq 0.5$, $\langle \text{sSFR} \rangle$ vanishes at $d_{\text{node}} \lesssim 1$ Mpc. The increase from low to high d_{node} is much more gradual at $z = 1$ ($\approx 3\times$ from $\langle d_{\text{node}} \rangle \sim 0.2$ Mpc to $\langle d_{\text{node}} \rangle \sim 15$ Mpc). At $z \geq 2$ however, there is virtually no dependence of $\langle \text{sSFR} \rangle$ on d_{node} . For intermediate-mass $9 \leq \log(M_*/M_\odot) < 10$ galaxies, the trends are similar in that there is a large ~ 1 dex rise in $\langle \text{sSFR} \rangle$ from the lowest to the highest d_{node} bin at $z = 0$, a much smaller rise at $z = 0.5$, and effectively no d_{node} dependence at $z \geq 1$. The lack of d_{node} -dependence of $\langle \text{sSFR} \rangle$ at $z > 1$ is also seen for high-mass $\log(M_*/M_\odot) \geq 10$ galaxies, but interestingly, these galaxies don’t show a monotonic increase in $\langle \text{sSFR} \rangle$ with d_{node} at lower redshifts. In fact, there is an *upturn* in $\langle \text{sSFR} \rangle$ at $d_{\text{node}} \lesssim 0.2$ Mpc following a rise with d_{node} at $d_{\text{node}} \gtrsim 0.2$ Mpc.

Considering the filament-centric relationships, we find

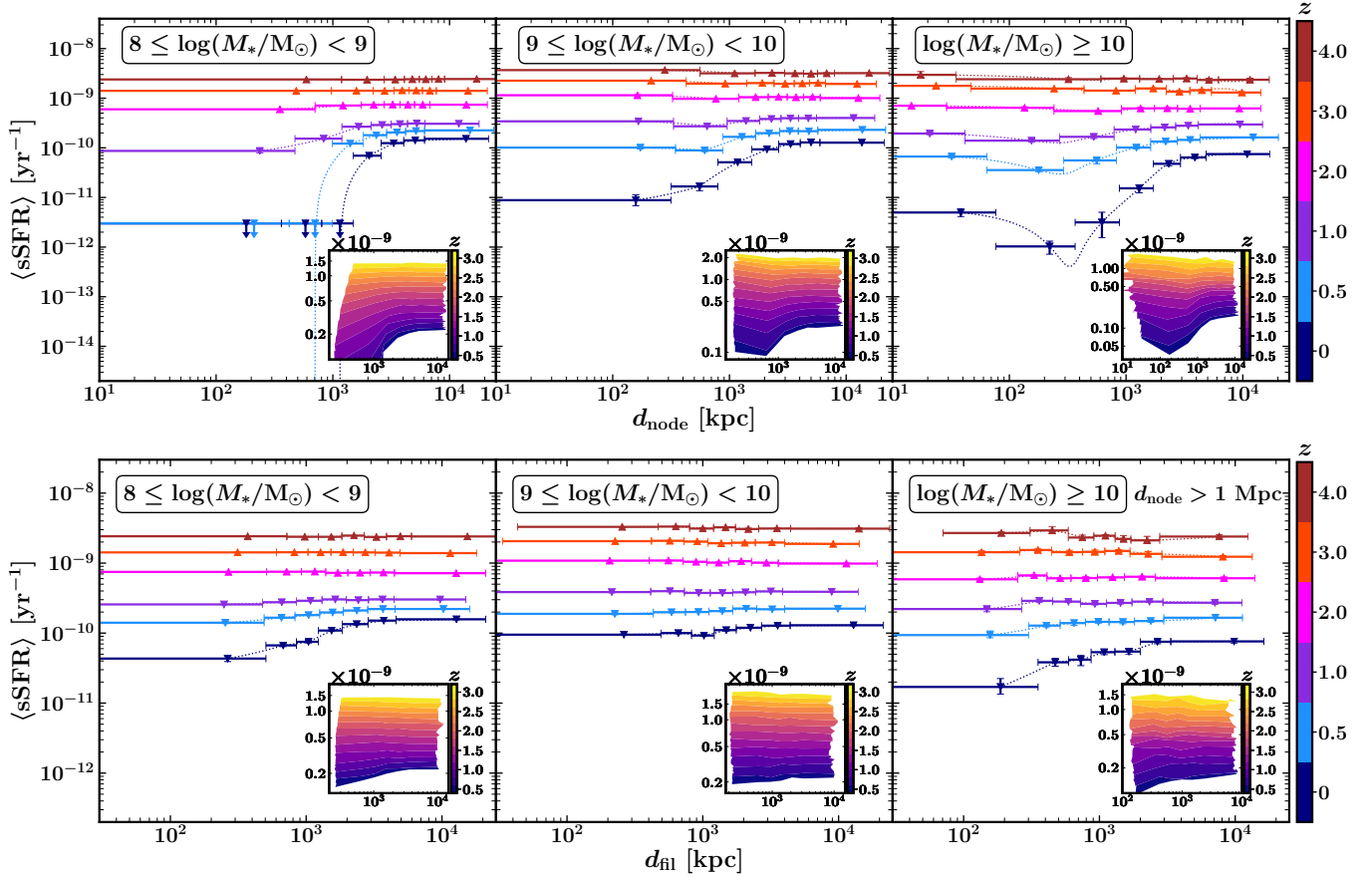


Figure 2. The median sSFR as a function of distance to the nearest node (top row) and filament spine (bottom row) for galaxies with $8 \leq \log(M_*/M_\odot) < 9$ (left panels), $9 \leq \log(M_*/M_\odot) < 10$ (middle panels), and $\log(M_*/M_\odot) \geq 10$ (right panels). The data points and curves are color-coded by redshift as indicated by the discrete color-bars on the right. Each panel contains an inset which is a continuous color contour plot showing the $\langle \text{sSFR} \rangle$ - d_{node} or $\langle \text{sSFR} \rangle$ - d_{fil} relationship for a larger number of intermediate redshifts, to help locate the redshift at which a distance-dependence disappears (see text). Only galaxies with $d_{\text{node}} > 1$ Mpc are included for the filament-centric relationships to mitigate the effects of potentially halo-centric effects from nearby clusters and groups. Note that some points are shown as upper limits on $\langle \text{sSFR} \rangle$. Star formation activity is dependent on d_{node} and (to a lesser extent) d_{fil} only at lower redshifts and disappears at $z \geq 2$.

both differences and similarities with the node-centric relationships. For low-mass galaxies at $z = 0$, there is a sizeable $\sim 5\times$ increase in $\langle \text{sSFR} \rangle$ from $\langle d_{\text{fil}} \rangle \sim 0.3$ Mpc to $\langle d_{\text{fil}} \rangle \sim 15$ Mpc, however the rise in $\langle \text{sSFR} \rangle$ with d_{fil} is negligible for $z \geq 0.5$. For the intermediate mass range, there is effectively no gradient of $\langle \text{sSFR} \rangle$ with d_{fil} at any redshift. For high-mass galaxies at $z = 0$, we do not see an upturn in $\langle \text{sSFR} \rangle$ at the lowest d_{fil} (unlike at low d_{node}) but rather a somewhat smooth rise of a few times in $\langle \text{sSFR} \rangle$ with d_{fil} from low to high d_{fil} . At $z > 0.5$, the relationship between $\langle \text{sSFR} \rangle$ and d_{fil} is again non-existent. Thus, only low-mass and high-mass galaxies at low redshifts are somewhat quenched near filaments, whereas this effect is almost ubiquitous near nodes.

One of the most striking findings on the star formation-cosmic web connection, seen in both the filament- and node-centric analyses, is the *disappearance of a dependence of star formation on distance to cosmic web structures at higher redshifts*. The color contour insets in Fig. 2 show the $\langle \text{sSFR} \rangle$ - d_{node} and $\langle \text{sSFR} \rangle$ - d_{fil} relationships for many

snapshots at $0.5 \leq z \leq 3$. These contours flatten out past a certain redshift for all three mass ranges, indicating that star formation activity is essentially independent of proximity to the cosmic web prior to this era. The independence of star formation on cosmic web node-centric distance occurs at $z \sim 1.3$ for $9 \leq \log(M_*/M_\odot) < 10$ galaxies and $z \sim 2$ for $8 \leq \log(M_*/M_\odot) < 9$ and $\log(M_*/M_\odot) \geq 10$ galaxies. The d_{fil} -independence of star formation occurs at $z \sim 1$ for low-mass and high-mass galaxies, while the star formation in moderate-mass galaxies does not show any significant d_{fil} -dependence at any redshift. From our analysis, it can be deduced that the cosmic web environment started affecting star formation activity during the latter stages of, or immediately after, the so-called “cosmic noon” of star formation when star formation rate density in the universe peaked (which ended around $z \sim 1.5$; e.g., [Madau & Dickinson 2014](#)).

3.2. Central And Satellite Galaxies

We separate our galaxy samples into central and satellite galaxies to understand how star formation is dependent on cosmic web environment for either galaxy type. At each red-

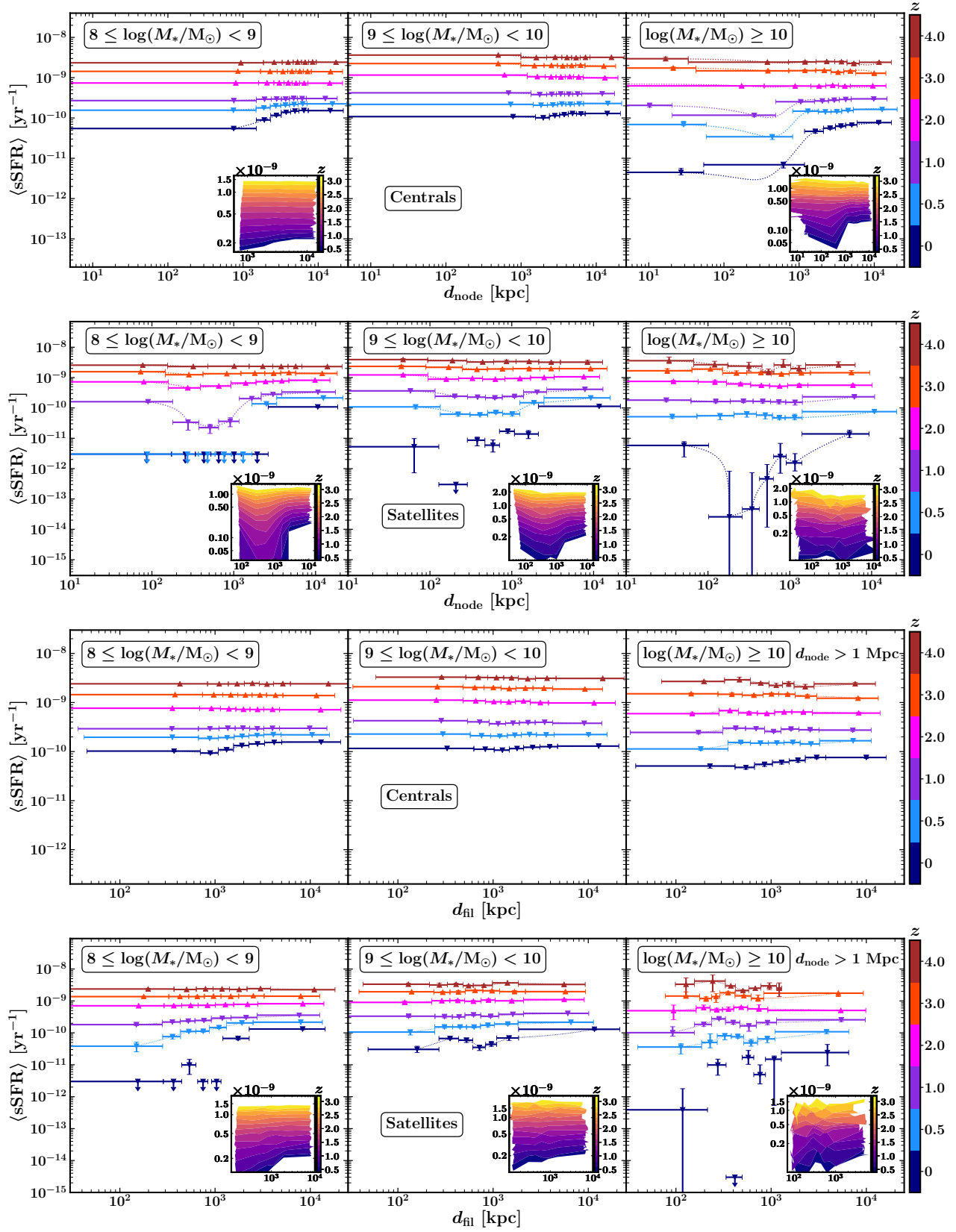


Figure 3. $\langle \text{sSFR} \rangle$ in bins of d_{node} (top two rows) and d_{fil} (bottom two rows) for central galaxies (1st and 3rd row) and satellite galaxies (2nd and 4th row) at different redshifts. Star formation in central galaxies appears to be less dependent on cosmic web environment than satellite galaxies which are significantly quenched at low d_{node} and d_{fil} at low redshifts. Neither centrals nor satellites exhibit a cosmic web-dependence of star formation activity at $z \geq 2$.

shift, we identify the most massive galaxy in a halo as central galaxies and the rest as satellite galaxies and then repeat the analysis in Section 3.1. The $\langle \text{sSFR} \rangle$ - d_{node} and $\langle \text{sSFR} \rangle$ - d_{fil} relationships are shown for central and satellite galaxies in Fig. 3. We only include the color contour inset plots in the panels where any significant relationship between cosmic web environment and star formation is seen.

In general, we find that star formation in satellite galaxies is strongly connected to cosmic web environment at low redshifts, whereas star formation in central galaxies is typically hardly affected (with the exception of high-mass centrals). At $z < 1$, there is a very modest rise in $\langle \text{sSFR} \rangle$ of low-mass centrals with d_{node} and in intermediate-mass centrals, there is no dependence of $\langle \text{sSFR} \rangle$ on d_{node} . In contrast, star formation is effectively quenched close to nodes in low-mass satellites at $z \leq 0.5$, and in intermediate-mass satellites at $z = 0$.

High-mass centrals show a strong correlation between $\langle \text{sSFR} \rangle$ and d_{node} at low redshifts. While the rise in $\langle \text{sSFR} \rangle$ with d_{node} is somewhat monotonic at $z = 0$, we see an upturn in $\langle \text{sSFR} \rangle$ at low d_{node} ($d_{\text{node}} \lesssim 0.1$ Mpc) at $z \sim 0.5 - 1$, similar to that found for the full galaxy population at the lowest redshifts (Fig. 2). This upturn is also seen in high-mass satellites at $z = 0$, suggesting that the elevation of star formation activity of high-mass galaxies very close to nodes is applicable for both centrals and satellites (with the caveat that the errors for the satellite relationships are higher). At higher d_{node} , there is a smooth rise in $\langle \text{sSFR} \rangle$ with d_{node} for satellites at $z \leq 0.5$ and for centrals at $z \leq 1$.

With respect to filaments, there is negligible dependence of $\langle \text{sSFR} \rangle$ on d_{fil} in centrals of any mass across cosmic time. Both low-mass and high-mass satellites are effectively quenched at low d_{fil} at $z = 0$, while the rise in $\langle \text{sSFR} \rangle$ with d_{fil} is more modest in intermediate-mass satellites. However the low-number statistics of the high-mass satellite population prevents us from drawing strong conclusions about their star formation dependence. While satellites appear to drive much of the dependence of star formation on proximity to cosmic web filaments and nodes at low redshifts, there is no statistically significant dependence of star formation on cosmic web environment at $z \geq 2$ for either centrals or satellites.

3.3. Gas Fraction And Cosmic Web Environment

To further investigate the star formation-cosmic web connection, we examine the available gas content in galaxies relative to proximity to nodes and filaments. To this end, we measure the galactic gas fraction,

$$f_{\text{gas}} = \frac{M_{\text{gas}}}{M_{\text{gas}} + M_*}, \quad (1)$$

which is the ratio of gas mass to sum of gas and stellar mass bound to a galaxy. We calculate the median gas fraction, $\langle f_{\text{gas}} \rangle$, in the same bins of d_{node} and d_{fil} for the same mass ranges and redshifts as above. We measure $\langle f_{\text{gas}} \rangle$ separately for all galaxies, centrals and satellites. The $\langle f_{\text{gas}} \rangle$ - d_{node} and $\langle f_{\text{gas}} \rangle$ - d_{fil} relationships are presented in Fig. 4 and Fig. 5, respectively. For clarity of presentation, we only include four redshift bins, $z = 0, 1, 2$, and 4 in these plots. As in Fig. 2, the $\pm 1\sigma$ bootstrapped error-bars on the medians are shown.

Fig. 4 shows that for the full galaxy population, there is a strong dependence of $\langle f_{\text{gas}} \rangle$ on d_{node} at lower redshifts. At $z = 0$, low-mass galaxies at $d_{\text{node}} \lesssim 1$ Mpc are completely devoid of gas, which explains why they are quenched in these environments. This is mostly driven by satellite galaxies, as low-mass centrals only see a drop of a few percent in $\langle f_{\text{gas}} \rangle$ from higher to lower d_{node} . In intermediate-mass galaxies, $\langle f_{\text{gas}} \rangle$ drops by an order of magnitude from the highest to the lowest d_{node} bin at $z = 0$, which is commensurate with the ~ 1 dex drop in $\langle \text{sSFR} \rangle$ in Fig. 2. This is again primarily driven by a dramatic decline in gas fraction of satellites while centrals only exhibit a modest decline.

In high-mass galaxies, we find a minimum in $\langle f_{\text{gas}} \rangle$ at $d_{\text{node}} \approx 0.7$ Mpc followed by a steep rise at lower d_{node} . This dramatic upturn in gas fraction helps explain the upturn in star formation at low d_{node} at low redshifts, but this turnover is a) much more pronounced in $\langle f_{\text{gas}} \rangle$ than in $\langle \text{sSFR} \rangle$ and b) persists out to $z = 3$ for $\langle f_{\text{gas}} \rangle$ while it only exists out to $z \sim 1$ for $\langle \text{sSFR} \rangle$. The relationship between $\langle f_{\text{gas}} \rangle$ and d_{node} in high-mass galaxies is largely dictated by central galaxies which experience high gas fractions close to nodes across cosmic time. This, however, does not result in highly enhanced star formation in low-redshift centrals at low d_{node} , implying a lack of star formation efficiency in these environments – possibly due to central AGN heating the gas in these galaxies and suppressing star formation (see discussion below). High-mass satellites also exhibit a small upturn in $\langle f_{\text{gas}} \rangle$ at $d_{\text{node}} \lesssim 0.1$ Mpc at $z \leq 3$. Unlike with star formation activity, the gas fraction in all $\log(M_*/M_\odot) \geq 10$ galaxies is dependent on proximity to nodes even at $z = 4$.

Proximity to filaments is less strongly correlated with $\langle f_{\text{gas}} \rangle$ than proximity to nodes, as shown in Fig. 5. At low redshifts, a monotonic rise in $\langle f_{\text{gas}} \rangle$ with d_{fil} in low and intermediate-mass galaxies is caused mostly by the steep rise in the satellite population, but this dependence disappears with increasing redshift. Centrals of all masses show virtually no d_{fil} -dependence on $\langle f_{\text{gas}} \rangle$ with at any redshift, consistent with a lack of dependence of star formation activity on distance to filaments.

We also note that the declining availability of gas in galaxies should not immediately result in reduced star formation activity, but instead there should be a time lag between the reduction in gas and the reduction in star formation. This is generally consistent with what we find: $\langle f_{\text{gas}} \rangle$ decreases with cosmic web proximity at higher redshift than $\langle \text{sSFR} \rangle$ does for any given stellar mass range. In some populations, such as satellites, a correlation between $\langle f_{\text{gas}} \rangle$ and d_{node} exists out to $z = 4$ while star formation is independent of d_{node} at $z \geq 2$. This potentially indicates that star formation is less efficient further from nodes at earlier times than closer to nodes.

Our results in this section suggest the following. 1) Star formation quenching near cosmic web structures is typically caused by scarcity of gas, 2) the gas fraction in satellite galaxies is more significantly affected by cosmic web environment than that in central galaxies, and drive the general cosmic web-dependence of gas fraction, and 3) at later times, high-mass galaxies, including both satellites and centrals, are more

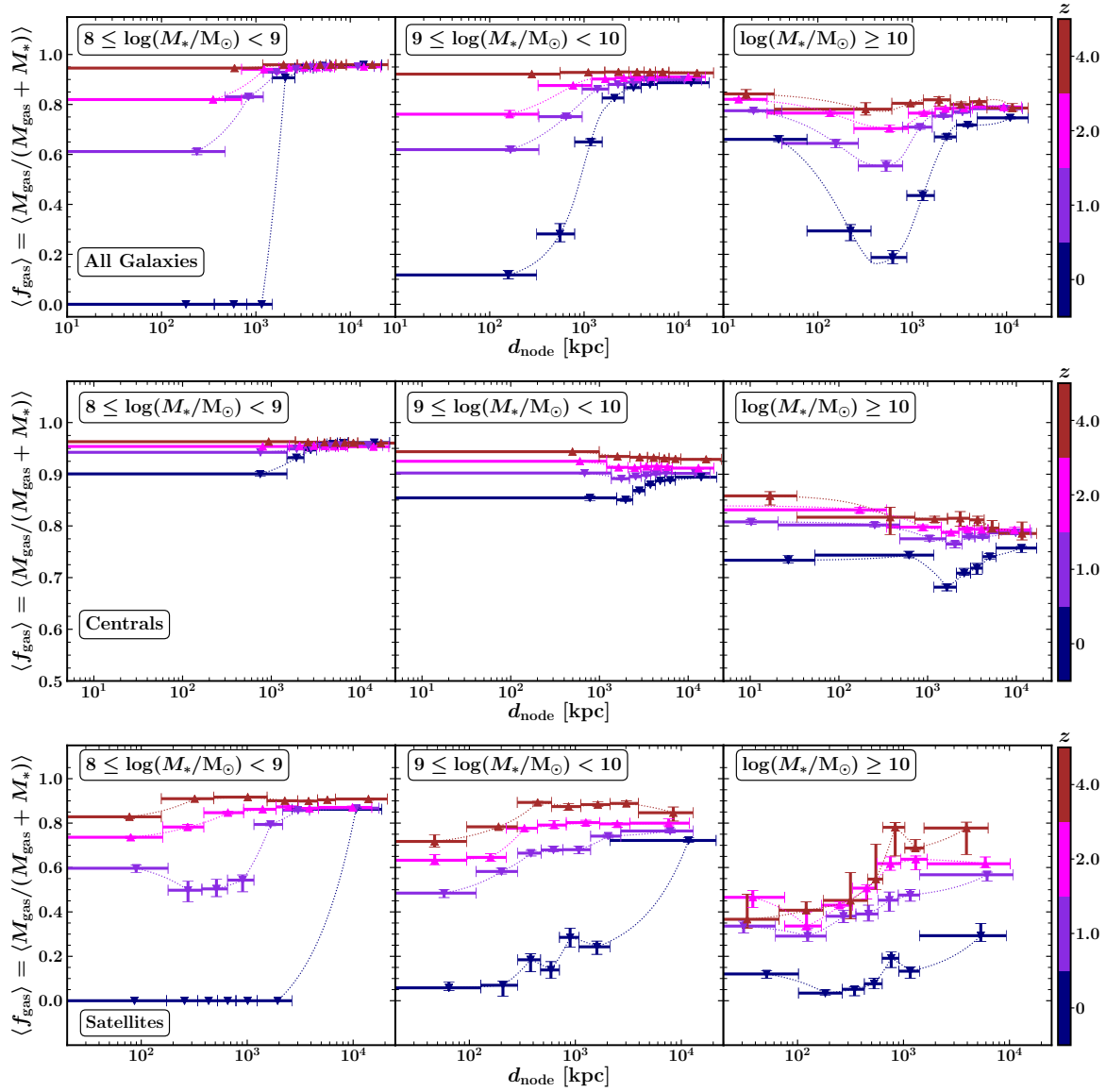


Figure 4. The median galactic gas fraction, $\langle f_{\text{gas}} \rangle$, as a function of d_{node} , for all galaxies (top row), centrals (middle row), and satellites (bottom row), at redshifts $z = 0, 1, 2$, and 4 . The general cosmic web-dependence of star formation follows from the available gas supply. Satellites drive the gas fraction trends for lower mass galaxies while both centrals and satellites drive the high-mass trends.

gas-rich near centers of nodes than at the outskirts, leading to increased star formation closer to nodes.

4. DISCUSSION

4.1. Physical Interpretations

Here, we interpret our results in terms of physical mechanisms governing the evolution of galaxies and large-scale structure. Perhaps the most puzzling result is that the star formation activity of galaxies in TNG do not depend on their large-scale cosmic web environment at $z \geq 2$, in contrast with later times when significant dependence occurs. At face value, this seems to suggest a rising importance of quenching driven by environment with cosmic time and indeed several recent works have found varying degrees of evidence for a lack of small or large-scale environmental dependence of star formation at higher redshifts (e.g., Moutard et al. 2018; Xu

et al. 2020; Chang et al. 2022; Momose et al. 2022).

4.1.1. The Cosmic Web-Dependence After Cosmic Noon

The low-redshift dependence of star formation activity on d_{node} and d_{fil} can generally be explained by the variation of gas fraction with these distances. In lower mass galaxies at low redshifts, the monotonic descent in $\langle \text{sSFR} \rangle$ with proximity to nodes and filaments is consistent with the corresponding descent in $\langle f_{\text{gas}} \rangle$. On average, low-mass galaxies that are within several hundred kpc of a node or filament effectively stop forming new stars at $z = 0$, most likely because they have very little to no gas available to do so, and this behavior is seen to be largely driven by satellites.

This points to a picture where dwarf galaxies that accrete on to the halos of more massive centrals are quenched in overdense environments where their gas supplies are depleted. Dwarf satellites located in galaxy clusters and groups

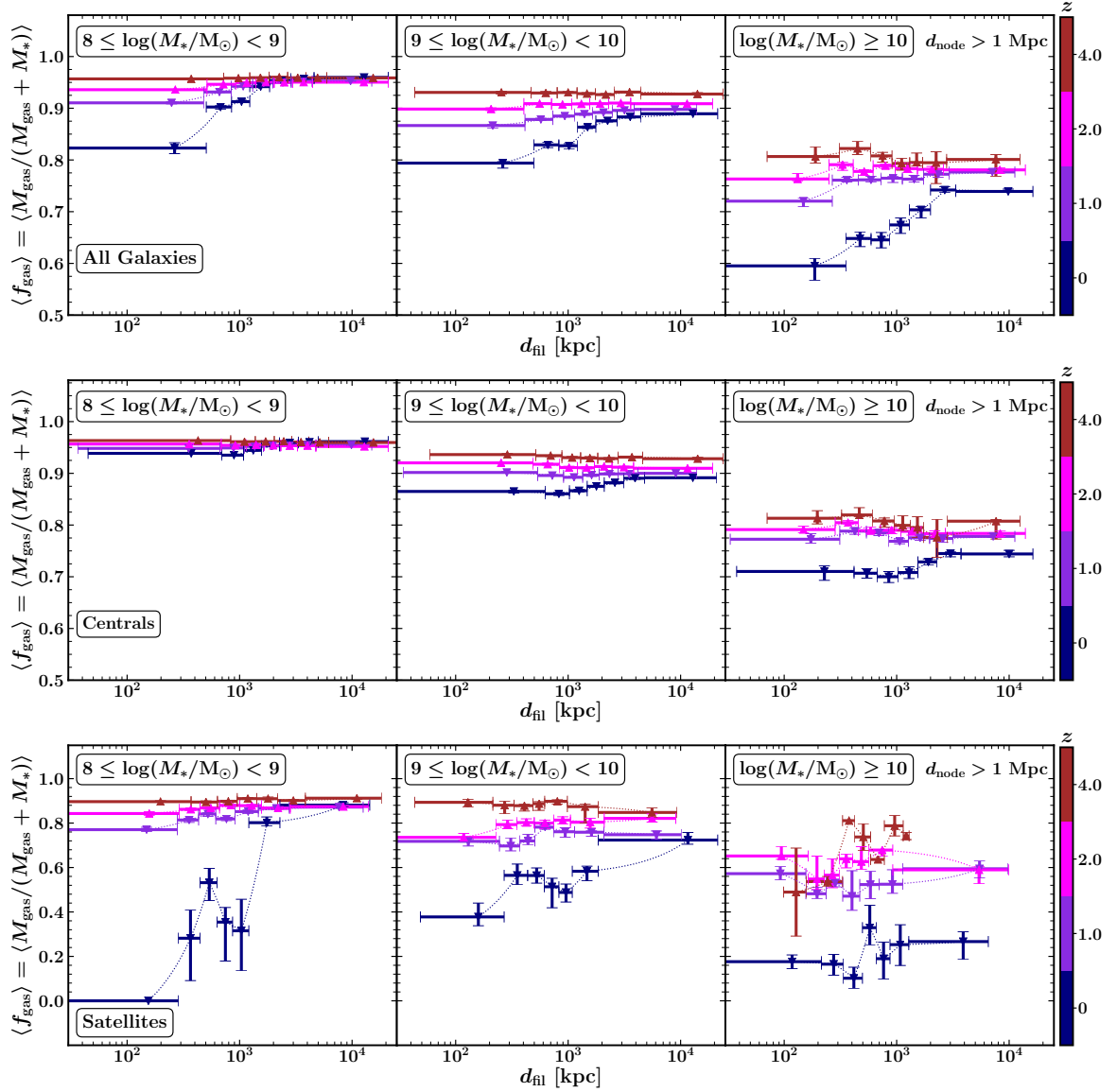


Figure 5. Same as Fig. 4, but in bins of d_{fil} . Satellites drive the dependence of $\langle f_{\text{gas}} \rangle$ on d_{fil} more than centrals.

are subjected to harsh gaseous environments dominated by warm and hot gas with high densities. In these environments, a combination of physical processes can act together on the star-forming ISM of dwarf satellites.

Gas can be removed by ram pressure stripping when these galaxies move through the group/cluster medium or by gravitational (tidal) interactions between the satellites and the central/other satellites or the halo itself. These processes, while often identified as the likely culprits for gas stripping and quenching of low-mass satellites in clusters/groups, typically act on relatively short timescales of $\lesssim 500$ Myr (e.g., Bahé & McCarthy 2015; Marasco et al. 2016). Here, we find that low-mass satellites close to nodes are already quenched at $z=0.5$ and have greatly reduced gas fractions at $z=1$, meaning that the quenched satellites in the local universe had been quenched much earlier. In fact, Donnari et al. (2021) found that in TNG, a large fraction of local $\log(M_*/M_\odot) \lesssim 10$ satellites in groups and clusters were members of other ha-

los whence they experienced environmental quenching before falling into their final host – a phenomenon dubbed “pre-processing” (see also, e.g., Hou et al. 2014).

AGN feedback from massive central galaxies in groups and clusters can also play an important role in quenching star formation in satellites. The TNG model allows for both “ejective”, or kinetic mode, feedback whereby BH expel star-forming gas from a galaxy and “preventative”, or thermal mode, feedback whereby BH heat up the gas and prevent star formation on longer timescales (Zinger et al. 2020). Both these modes of AGN feedback have been observed in galaxies near and far (e.g., Fabian 2012; King & Pounds 2015). In particular, Martín-Navarro et al. (2019) showed that stronger BH feedback produces hotter group/cluster media that makes quenching more efficient in satellites. While beyond the scope of this work, it would be valuable to understand how central BH properties such as mass and accretion rate could explain the cosmic web-dependence of star formation.

Satellites at low filament-centric distances and $d_{\text{node}} > 1$ Mpc would reside in more intermediate density environments than those at low node-centric distances. In either of these types of environments, fresh gas accretion on to the ISM can be halted by strangulation/starvation such that star formation ceases over longer timescales of $\sim \text{few Gyr}$ (e.g., Peng et al. 2015; Zinger et al. 2018). In a comprehensive analysis of nearby galaxies, Trussler et al. (2020) found that starvation is likely to be the initial prerequisite for quenching across virtually all masses but the remaining cold ISM gas needs to be heated or ejected to complete the quenching process. Low-mass centrals, on the other hand, do not exhibit much of a cosmic web-dependence on gas fraction and consequently, star formation. For these galaxies, so-called “mass quenching” via internal processes (such as feedback) is dominant over environmental effects (e.g., Peng et al. 2010).

In our investigation, we only considered the gas bound to a galaxy and not that which is bound to the *halo*, i.e., the CGM. Regardless, we find that the galactic gas fraction of low-mass satellites declines dramatically from $z = 1$ to $z = 0$ at low d_{node} and to a lesser but still significant extent at low d_{fil} , indicating either a lack of accretion from the IGM to the CGM or from the CGM to the ISM. In regards to the former mechanism, hydrodynamical simulations show that accretion of cold gas from the IGM becomes increasingly inefficient over time (e.g., Anglés-Alcázar et al. 2017). As for the latter, gas in the CGM may be heated substantially or even ejected by SNe (e.g., Pandya et al. 2022) or AGN (as discussed above) to prevent accretion on to the ISM. We also did not measure the fraction of *cool* gas which would in principle be a more direct measure of gas supply available for star formation.

In low-redshift $\log(M_*/M_\odot) \geq 10$ galaxies, there is a minimum in gas fraction and star formation activity at $d_{\text{node}} \sim 0.2$ Mpc, following an unexpected rise at lower d_{node} . This upturn in f_{gas} and sSFR close to nodes persists out to $z = 2$, but manifests in an analogous relationship between star formation and proximity to nodes at $z \leq 1$. When we limit our sample to even higher mass galaxies, this effect is further accentuated, implying that the highest mass galaxies are primarily responsible. The effect of enhanced star formation very close to nodes is stronger in satellites than in centrals at $z = 0$ while the converse is true at $z = 0.5 - 1$. The fact that both $\langle \text{sSFR} \rangle$ and $\langle f_{\text{gas}} \rangle$ are lowest at $d_{\text{node}} \sim 0.2$ Mpc implies that massive galaxies falling into groups/clusters from the outskirts are more gas-poor and passive relative to galaxies at the center.

It is conceivable that some/much of the gas removed from low-mass satellites in rich groups and clusters end up in higher mass galaxies which enable the latter populations to form stars at higher rates near the centers of these halos. The cores of many groups and clusters have been observed to be abundant in cold gas which may temporarily trigger star formation near the center (e.g., McDonald et al. 2012; Olivares et al. 2019). However, this gas is hypothesized to feed central AGN activity and eventually curtail star formation (see Donahue & Voit 2022, and references therein). Heating from

the central AGN could explain why the rise in star formation at low d_{node} is not as dramatic as the rise in gas fraction in high-mass galaxies.

The enhancement of star formation in dense environments is not typically observed in statistical studies of the cosmic web-galaxy connection (e.g., Kraljic et al. 2018; Winkel et al. 2021). But there is evidence – both in observations (e.g., Roediger et al. 2014) and in simulations (e.g., Nelson et al. 2018) – of galaxies in groups/clusters enjoying brief episodes of star formation via compression of gas from ram pressure stripping, mergers or other processes, a phenomenon sometimes called “rejuvenation.” However, these events are rare in TNG, with only 10% of $\log(M_*/M_\odot) > 11$ galaxies and 6% of all galaxies at $z = 0$ ever having experienced them (Nelson et al. 2018). A large analysis of satellite galaxies by Martín-Navarro et al. (2021) showed that AGN outflows can clear out the CGM of massive halos, which reduces ram pressure and preserves star formation in satellites along the direction of the outflows (the minor axis of the central). These phenomena of *positive* AGN feedback can potentially boost star formation in dense environments such as those close to nodes.

It is also possible that the high-density upturn in star formation is a result of some additional mechanism in the simulations funnelling too much gas into galaxies, over-cooling the gas, or otherwise reducing the efficiency of quenching at the highest density environments. Donnari et al. (2021) report that TNG galaxies in dense environments have diverse histories and quenching pathways that may complicate the interpretation of how and when they quench. Moreover, the AGN-driven gas expulsion in TNG is known to be so efficient that there are very few galaxies with intermediate sSFR (i.e., Green Valley galaxies; e.g., Schawinski et al. 2014), creating tension with observations (Terrazas et al. 2020).

4.1.2. No Cosmic Web-Dependence Before Cosmic Noon?

There is now a growing body of evidence suggesting that cosmological accretion shocks from the formation of cosmic web structures, similar to those around massive halos, can affect galaxy formation. Birnboim et al. (2016) showed that in filaments with a specific linear mass density, the accretion shocks are unstable. These structures can efficiently siphon cool gas into $10 \lesssim \log(M_{200,c}/M_\odot) \lesssim 13$ halos at $z = 3$ and $12 \lesssim \log(M_{200,c}/M_\odot) \lesssim 15$ halos at $z = 0$ (see their Fig. 5). According to the stellar-to-halo-mass relations at these redshifts (e.g., Behroozi et al. 2019), this means that unstable filaments can potentially enhance star formation in galaxies of virtually all masses we studied at higher redshifts, while at lower redshifts only the most massive galaxies would see an increase in star formation via this channel. This phenomenon is a possible pathway for early galaxies close to filaments and nodes to have their sSFR elevated to levels comparable to those far from filaments and nodes.

This explanation necessitates an environmental dependence of *overall star formation activity* at high z instead of specifically *quenching*. The net trend of constant sSFR with distance from cosmic web structures could be naively interpreted as quenching processes being environment-

independent at high z . As noted in Section 3.3, we find evidence of star formation in satellites close to nodes being more efficient than those further away at early times ($z \geq 2$). A plausible scenario for this is that gas is more efficiently channelled into the centers of nodes, and eventually galaxies, via cold streams at high redshift (e.g., Dekel et al. 2009).

Cosmological accretion shocks can also suppress star formation in galaxies. Zinger et al. (2018) showed that accretion shocks at the outskirts of galaxy clusters can quench satellites, which likely impact galaxies near nodes in our analysis. In TNG, Li et al. (2023) found that shock-induced stripping of the ISM and CGM can quench low-mass satellites inside clusters at $z < 0.11$. Recently, Pasha et al. (2022) found that $5.5 < \log(M_*/M_\odot) < 8.5$ central galaxies at $z = 2 - 5$ can be quenched by shock-heated cosmic sheets (which eventually collapse into filaments and nodes; e.g., Bond et al. (1996)). These shocks directly raise the ambient gas temperature in the vicinity of the sheets and suppress gas accretion and star formation in surrounding galaxies.

The impact of accretion shocks in filaments and nodes on galaxy quenching, as a function of both stellar mass and redshift, may be profound in interpreting the results of this paper and therefore deserve detailed investigation. In a follow-up study, we will address this problem by analyzing the gaseous conditions of filaments and nodes – with particular emphasis on accretion shock signatures – in tandem with properties of the galaxies residing within them across cosmic time. This analysis will also allow us to characterize filaments and nodes in more detail and account for the fact that not all filaments or nodes will have the same effect on galaxy formation (e.g., Galárraga-Espinosa et al. (2020) found short and long filaments in TNG to be statistically different populations).

4.1.3. Other Important Physical Considerations

Angular momentum is another important aspect of galaxy formation which may shed additional light on how quenching is affected by the cosmic web. From their analysis of quenching timescales in TNG, Walters et al. (2022) suggested that the angular momentum of accreting gas is a vital factor in determining how quickly galaxies quench. In the cosmic web framework, galaxies form in the vorticity-rich regions of filaments, acquire angular momentum, and drift to the nodes (e.g., Dubois et al. 2014; Codis et al. 2015). Simulations have predicted for many years that at $z \gtrsim 1.5$, gas is funnelled through cold filamentary streams into the centers of galaxies which transfers some of the angular momentum to the galaxy (e.g., Dekel et al. 2009; Pichon et al. 2011). Over time as these streams disappear due to heating or other processes, efficiency of galaxy formation at the centers of filaments and nodes may also decline, potentially explaining the difference in star formation activity in these regions between low and high redshift. Additionally, galactic properties such as mass and sSFR have been found to be correlated with the acquisition of angular momentum from the cosmic web (e.g., Kraljic et al. 2019; Welker et al. 2020). Thus, a complete understanding of how the cosmic web affects quenching needs to account for angular momentum acquisition in galaxies in

tandem with proximity to cosmic web structures.

Many of the relationships between star formation and cosmic web environment may result from the assembly of DM halos. Subhalo abundance matching predictions from Λ CDM cosmology are found to agree with observed SDSS galaxy distributions, implying that the local density-dependence of galaxy properties stems from the corresponding density-dependence of halo properties (Dragomir et al. 2018). In the Bolshoi-Planck simulations, Lee et al. (2017) found that in $\log(M_{200,c}/M_\odot) \lesssim 12$ halos, halo accretion is higher in low-density environments at $z \lesssim 1$ and in high-density environments at $z \gtrsim 1$. However, some N -body simulations have shown that DM halo properties are independent of cosmic web location at fixed overdensities (e.g., Goh et al. 2019). A detailed analysis of the dependence of halo mass accretion with cosmic web environment in TNG is necessary to disentangle the effect of halo mass growth from baryonic effects in determining the galaxy quenching-cosmic web connection.

4.2. Other Caveats

We consider some other aspects of our methodology which may affect the robustness of our results as well as the conclusions we draw. The first is how numerical resolution in the simulation may affect our results. Galárraga-Espinosa et al. (2021) showed that despite the ~ 8 times difference in resolution between TNG300-1 and TNG300-2, there are only minor differences in the distribution (including the DISPERSE reconstruction) and properties of filaments. The large scales of the cosmic web are likely to be well-resolved with any of the TNG runs, but the smaller scales of galaxy formation are more sensitive to resolution. Thus, it would be interesting to compare our results for TNG100-1 with those of TNG50-1, which has ~ 16 times the particle mass resolution of TNG100-1 (e.g., Nelson et al. 2019a, 2020).

The input physics model is another potential source of uncertainty for theoretical galaxy evolution studies. Galárraga-Espinosa et al. (2020) found that different baryonic physics implemented in different simulations result in somewhat different matter distribution around filaments but that gravity is still the dominant driver. Xu et al. (2020) investigated the sSFR of galaxies in filaments, nodes, sheets, and voids in the EAGLE simulation which uses somewhat different hydrodynamics and feedback prescriptions from the TNG model (see Schaye et al. 2015). They found that at $z < 1$, galaxies with $\log(M_*/M_\odot) \lesssim 10.5$ are less star-forming in nodes than other cosmic web environments, while for more massive galaxies there is virtually no cosmic web-dependence. At $z > 1$, they found that there is statistically no dependence of the cosmic web environment on sSFR, consistent with our findings. It would be interesting to apply our methodology to investigate the evolving cosmic web-dependence of star formation in other hydrodynamical cosmological simulations such as SIMBA (Davé et al. 2019) and Horizon-AGN (Dubois et al. 2014). Such comparisons might help illuminate the effect of uncertain baryonic processes such as AGN feedback on the relationship between galaxy formation and the cosmic web.

Another crucial check on our results is the cosmic web reconstruction itself. As mentioned in Section 2.2, we experimented with DISPERSE parameter choices such as persistence and smoothing of the filamentary skeleton. The latter did not have any significant effect on our results whatsoever and the effect of varying the former was on the frequency of the identified structures but not on any of the qualitative conclusions we report. Overall, we consider our results to be robust to parameter choices. There are several other cosmic web reconstruction techniques that have been employed for cosmic web studies, which have advantages and disadvantages over the DISPERSE framework (see Libeskind et al. 2018, for a detailed comparison of many of these methods). We are applying a new state-of-the-art cosmic web reconstruction algorithm called the Monte Carlo Physarum Machine (MCPM) inspired by the *Physarum Polycephalum* (slime mold) organism (Elek et al. 2021, 2022) to compare to the local density estimation and global cosmic web characterization from DISPERSE. This method produces continuous cosmic matter densities (as opposed to discrete DTFE densities at the locations of galaxies) and has been applied successfully to both theoretical and observational datasets (e.g., Burchett et al. 2020; Simha et al. 2020; Wilde et al. 2023).

We also assess the importance of local galaxy overdensity in shaping the star formation-cosmic web connection. We repeat our analyses in Section 3 by only considering galaxies with local DTFE galaxy overdensity (as computed by DISPERSE) within $\pm 1\sigma$ of the mean. We find that the resulting relationships with respect to d_{node} and d_{fil} look strikingly similar to those we report without filtering out galaxies by overdensity, implying that the effect of cosmic web environment on star formation persists beyond just the highest density regions of the universe. However, we stress that local overdensity and global cosmic web environment are necessarily related to each other and therefore it is not trivial to disentangle the effect of one from another. We defer a detailed characterization of the dependence of d_{fil} and d_{node} on overdensity across different redshifts in TNG-100 to a future work (see Malavasi et al. 2022, for an in-depth mapping of overdensity to cosmic web proximity in TNG-300).

Finally, in our interpretations we neglected the effect of pseudo-evolution of filaments and nodes, i.e., evolution of the reference density (in our case, the DTFE mean density) instead of a true *physical* density. Such pseudo-evolution is known to strongly drive the mass-evolution in DM halos, especially at lower redshifts (Diemer et al. 2013), and we defer a detailed investigation of this effect to future work.

4.3. Testing Predictions with Observations

The predictions presented herein from the TNG-100 simulation establish clear objectives for observational studies. First, we identified a point in cosmic time where galaxies' star formation activity begins depending on their location relative to the large-scale cosmic web environment. Confronting this prediction with observations will necessitate wide-field galaxy surveys capable of characterizing the large-scale structure over a large range of redshifts, out to at least

$z = 2$. Second, a common theme we observed in both sSFR and gas fraction were increases at small node-centric distances for high-mass galaxies. This will require both the extensive survey data necessary for the first finding and, perhaps even more challenging, measurements of the gas contents of these galaxies. Spectroscopic galaxy surveys both underway and planned for the next several years should make serious headway towards at least the first element of this challenging observational experiment.

The current gold standard for wide-field spectroscopic surveys is SDSS, which can provide the lowest redshift anchor point for such a comparison. The quoted SDSS spectroscopic completeness limit of $m_r = 17.7$ would correspond to a redshift limit of $z \sim 0.01$ for the lowest mass galaxies studied here ($10^8 M_\odot$). Even at $z \sim 0.1$, SDSS is only complete to $\sim 10^{10} M_\odot$, covering the most massive bin we study. Thus, SDSS, in principle, is capable of yielding measurements comparable with the dark blue data points in Figures 2 and 3. Although an independent analysis of observational datasets with our methodology is beyond the scope of this paper, we refer the reader to the work of Kuutma et al. (2017), Crone Odekon et al. (2018), and Winkel et al. (2021), who explore similar relationships with SDSS. Also of note is Kraljic et al. (2018) who employ the Galaxy and Mass Assembly (GAMA) survey, which goes two magnitudes deeper than SDSS albeit over a much smaller volume. Still, this does not push completeness to the $z > 1$ transition point in cosmic web dependence we report here.

Constraining the higher redshifts will be more difficult, although the various Dark Energy Spectroscopic Instrument (DESI) surveys should enable cosmic web reconstructions at intermediate redshifts. Initial data and results from the Survey Validation phase are beginning to be released now, showing promising prospects for mapping the large-scale structure to $z \sim 0.5$ for the Bright Galaxy Survey, $z \sim 1.1$ for the Luminous Red Galaxies (LRGs), $z \sim 1.6$ for Emission Line Galaxies (ELGs), and possibly beyond (Lan et al. 2023, and references therein). However, each of these samples is likely to contain highly biased tracers of the underlying structure; e.g., the LRGs are by definition passive galaxies and will preferentially reside in the most massive halos, likely tracing nodes. Conversely, the ELGs, being vigorously star-forming, might bias against these very environments. Nevertheless, neither of these samples will suitably represent the full diversity in star formation exhibited by the general population. Deep follow-up surveys with more agnostic selection criteria will be necessary for a fair comparison with our results.

Spectroscopic surveys with *JWST* and, eventually, the *Nancy Grace Roman Space Telescope* will yield galaxy datasets ripe for placing in context with the cosmic web mapped by DESI. *Roman*, which will map 1700 deg^2 of the sky at infrared wavelengths via the High Latitude Spectroscopic Survey (Wang et al. 2022), should reveal the cosmic web over scales of $\sim 1 \text{ Gpc}$ as well as the galaxies within to $z \sim 2$. In the shorter term, *JWST*, through programs such as JADES (Cameron et al. 2023), will yield galaxy spectra to $z > 5$ albeit over much smaller fields of view (the *JWST*

Micro-shutter Assembly will map scales ~ 1 Mpc across in a single pointing). An amalgamation of several such deep fields will be necessary to mitigate cosmic variance.

5. CONCLUSION

In this study, we investigated the IllustrisTNG simulations to understand how the star formation activity of galaxies depends on their cosmic web environment. We used all $\log(M_*/M_\odot) \geq 8$ galaxies to reconstruct the cosmic web in each of the TNG-100 snapshots using the DISPERSE framework. We measured the median sSFR and median f_{gas} of galaxies as a function of distance to the nearest cosmic web node (d_{node}) and filament spine (d_{fil}). Our main results are as follows:

1. The $\langle \text{sSFR} \rangle$ of galaxies at any mass only depends on d_{node} or d_{fil} at redshifts $z \lesssim 2$; *the median star formation is independent of cosmic web environment at $z \geq 2$* . This holds true also for central and satellite galaxies separately.
2. In $\log(M_*/M_\odot) < 10$ galaxies, $\langle \text{sSFR} \rangle$ increases monotonically with d_{node} at $z \leq 1$, with $8 \leq \log(M_*/M_\odot) < 9$ galaxies being completely quenched at $d_{\text{node}} < 1$ Mpc at $z \leq 0.5$. $\langle \text{sSFR} \rangle$ has a shallower increase with d_{fil} at these redshifts. These trends are almost entirely driven by satellites.
3. In $\log(M_*/M_\odot) \geq 10$ galaxies, the $\langle \text{sSFR} \rangle$ - d_{node} relationship inverts at $d_{\text{node}} \lesssim 0.1$ Mpc up to $z = 1$, while the $\langle \text{sSFR} \rangle$ - d_{fil} relation does not. The $\langle \text{sSFR} \rangle$ - d_{node} inversion is driven by both satellites and centrals, but the $\langle \text{sSFR} \rangle$ - d_{fil} relationship is due to satellites.
4. Most of these star formation-cosmic web relationships can be explained by the cosmic web-dependence of gas fraction in galaxies, although there is evidence of $\langle f_{\text{gas}} \rangle$ depending more strongly on cosmic web environment than $\langle \text{sSFR} \rangle$ in some cases.

Our results point to a picture where the influence of the cosmic web environment on quenching galaxies is first established at $z \sim 2$. In the last ~ 10 Gyr, low-mass dwarf satellites

are quenched by their star-forming gas supplies being depleted either on short timescales (e.g., via ram pressure stripping or outflows) or on longer timescales (e.g., via starvation), while low-mass centrals are quenched more by internal processes rather than their cosmic web environment. At this epoch, high-mass galaxies at the centers of nodes are more gas-rich and star-forming than their counterparts at the outskirts, which could be due to temporary rejuvenation events, positive AGN feedback, or a consequence of the TNG model itself. In the earlier universe (>10 Gyr ago), cosmic web structures likely aided star formation more than they suppressed it, possibly via unstable filaments feeding cold gas to galaxies or cold streams efficiently funnelling high-angular momentum gas to the central regions of filaments and nodes.

In a follow-up study, we will analyze the gas particles in TNG-100 to understand how the gaseous conditions of filaments and nodes affect galaxy formation, in particular how accretion shocks around filaments and nodes affect star formation. Furthermore, we will compare the cosmic web reconstruction from DISPERSE with that from the novel MCPM algorithm (Elek et al. 2021, 2022) to obtain more fine-grained insights into the global and local environmental dependence of star formation across cosmic time. The results of this work provide important predictions to test against ongoing large spectroscopic surveys such as SDSS and DESI, as well as those ongoing and planned with *JWST* and *Roman*.

We are very grateful to N. Luber and Z. Edwards for help with setting up DISPERSE. We thank attendees of the 2022 Santa Cruz Galaxy Workshop and the 2023 KITP Cosmic Web Conference, including F. van den Bosch, J. Woo, H. Aung, J. Powell, C. Pichon, U. Kuchner, C. Welker, S. Simha, K.-G. Lee, and R. Momose, for stimulating and interesting conversations on this work. FH, JNB, and AA are supported by the National Science Foundation LEAPS-MPS award #2137452. OE is supported by an incubator fellowship of the Open Source Program Office at UC Santa Cruz funded by the Alfred P. Sloan Foundation (G-2021-16957). DN is supported by NSF (AST-2206055) and NASA (80NSSC22K0821 & TM3-24007X) grants.

REFERENCES

- Anglés-Alcázar, D., Faucher-Giguère, C.-A., Kereš, D., et al. 2017, *MNRAS*, **470**, 4698
- Aragon Calvo, M. A., Neyrinck, M. C., & Silk, J. 2019, *The Open Journal of Astrophysics*, **2**, 7
- Bahé, Y. M., & McCarthy, I. G. 2015, *MNRAS*, **447**, 969
- Balogh, M. L., & Morris, S. L. 2000, *MNRAS*, **318**, 703
- Behroozi, P., Wechsler, R. H., Hearin, A. P., & Conroy, C. 2019, *MNRAS*, **488**, 3143
- Birnboim, Y., & Dekel, A. 2003, *MNRAS*, **345**, 349
- Birnboim, Y., Padnos, D., & Zinger, E. 2016, *ApJL*, **832**, L4
- Bluck, A. F. L., Maiolino, R., Sánchez, S. F., et al. 2020, *MNRAS*, **492**, 96
- Bond, J. R., Kofman, L., & Pogosyan, D. 1996, *Nature*, **380**, 603
- Boselli, A., Fossati, M., & Sun, M. 2022, *A&A Rv*, **30**, 3
- Boselli, A., & Gavazzi, G. 2006, *PASP*, **118**, 517
- Brinchmann, J., Charlot, S., White, S. D. M., et al. 2004, *MNRAS*, **351**, 1151
- Burchett, J. N., Elek, O., Tejos, N., et al. 2020, *ApJL*, **891**, L35
- Cameron, A. J., Saxena, A., Bunker, A. J., et al. 2023, *arXiv e-prints*, [arXiv:2302.04298](https://arxiv.org/abs/2302.04298)

- Cattaneo, A., Dekel, A., Devriendt, J., Guiderdoni, B., & Blaizot, J. 2006, *MNRAS*, **370**, 1651
- Chang, W., Fang, G., Gu, Y., et al. 2022, *ApJ*, **936**, 47
- Codis, S., Pichon, C., & Pogosyan, D. 2015, *MNRAS*, **452**, 3369
- Crone Odekon, M., Hallenbeck, G., Haynes, M. P., et al. 2018, *ApJ*, **852**, 142
- Croton, D. J., Springel, V., White, S. D. M., et al. 2006, *MNRAS*, **365**, 11
- Darvish, B., Mobasher, B., Sobral, D., et al. 2016, *ApJ*, **825**, 113
- Darvish, B., Sobral, D., Mobasher, B., et al. 2014, *ApJ*, **796**, 51
- Davé, R., Anglés-Alcázar, D., Narayanan, D., et al. 2019, *MNRAS*, **486**, 2827
- Dekel, A., & Birnboim, Y. 2006, *MNRAS*, **368**, 2
- Dekel, A., Birnboim, Y., Engel, G., et al. 2009, *Nature*, **457**, 451
- Diemer, B., More, S., & Kravtsov, A. V. 2013, *ApJ*, **766**, 25
- Dolag, K., Borgani, S., Murante, G., & Springel, V. 2009, *MNRAS*, **399**, 497
- Donahue, M., & Voit, G. M. 2022, *PhR*, **973**, 1
- Donnari, M., Pillepich, A., Joshi, G. D., et al. 2021, *MNRAS*, **500**, 4004
- Dragomir, R., Rodríguez-Puebla, A., Primack, J. R., & Lee, C. T. 2018, *MNRAS*, **476**, 741
- Dubois, Y., Pichon, C., Welker, C., et al. 2014, *MNRAS*, **444**, 1453
- Eardley, E., Peacock, J. A., McNaught-Roberts, T., et al. 2015, *MNRAS*, **448**, 3665
- Elbaz, D., Daddi, E., Le Borgne, D., et al. 2007, *A&A*, **468**, 33
- Elek, O., Burchett, J. N., Prochaska, J. X., & Forbes, A. G. 2021, *IEEE Transactions on Visualization and Computer Graphics*, **27**, 806-816
- . 2022, *Artificial Life*, **28**
- Fabian, A. C. 2012, *ARA&A*, **50**, 455
- Gabor, J. M., & Davé, R. 2012, *MNRAS*, **427**, 1816
- Galárraga-Espinosa, D., Aghanim, N., Langer, M., Gouin, C., & Malavasi, N. 2020, *A&A*, **641**, A173
- Galárraga-Espinosa, D., Aghanim, N., Langer, M., & Tanimura, H. 2021, *A&A*, **649**, A117
- Goh, T., Primack, J., Lee, C. T., et al. 2019, *MNRAS*, **483**, 2101
- Hou, A., Parker, L. C., & Harris, W. E. 2014, *MNRAS*, **442**, 406
- Kereš, D., Katz, N., Fardal, M., Davé, R., & Weinberg, D. H. 2009, *MNRAS*, **395**, 160
- Kereš, D., Katz, N., Weinberg, D. H., & Davé, R. 2005, *MNRAS*, **363**, 2
- King, A., & Pounds, K. 2015, *ARA&A*, **53**, 115
- Kotecha, S., Welker, C., Zhou, Z., et al. 2022, *MNRAS*, **512**, 926
- Kraljic, K., Arnouts, S., Pichon, C., et al. 2018, *MNRAS*, **474**, 547
- Kraljic, K., Pichon, C., Dubois, Y., et al. 2019, *MNRAS*, **483**, 3227
- Kuutma, T., Tamm, A., & Tempel, E. 2017, *A&A*, **600**, L6
- Laigle, C., Pichon, C., Arnouts, S., et al. 2018, *MNRAS*, **474**, 5437
- Lan, T.-W., Tojeiro, R., Armengaud, E., et al. 2023, *ApJ*, **943**, 68
- Larson, R. B., Tinsley, B. M., & Caldwell, C. N. 1980, *ApJ*, **237**, 692
- Lee, C. T., Primack, J. R., Behroozi, P., et al. 2017, *MNRAS*, **466**, 3834
- Li, H., Wang, H., Mo, H. J., et al. 2023, *ApJ*, **942**, 44
- Libeskind, N. I., van de Weygaert, R., Cautun, M., et al. 2018, *MNRAS*, **473**, 1195
- Madau, P., & Dickinson, M. 2014, *ARA&A*, **52**, 415
- Malavasi, N., Langer, M., Aghanim, N., Galárraga-Espinosa, D., & Gouin, C. 2022, *A&A*, **658**, A113
- Marasco, A., Crain, R. A., Schaye, J., et al. 2016, *MNRAS*, **461**, 2630
- Martín-Navarro, I., Burchett, J. N., & Mezcua, M. 2019, *ApJL*, **884**, L45
- Martín-Navarro, I., Pillepich, A., Nelson, D., et al. 2021, *Nature*, **594**, 187
- McDonald, M., Bayliss, M., Benson, B. A., et al. 2012, *Nature*, **488**, 349
- Momose, R., Lee, K.-G., Horowitz, B., Ata, M., & Kartaltepe, J. S. 2022, *arXiv e-prints*, [arXiv:2212.05984](https://arxiv.org/abs/2212.05984)
- Moutard, T., Sawicki, M., Arnouts, S., et al. 2018, *MNRAS*, **479**, 2147
- Nelson, D., Pillepich, A., Springel, V., et al. 2018, *MNRAS*, **475**, 624
- . 2019a, *MNRAS*, **490**, 3234
- Nelson, D., Springel, V., Pillepich, A., et al. 2019b, *Computational Astrophysics and Cosmology*, **6**, 2
- Nelson, D., Sharma, P., Pillepich, A., et al. 2020, *MNRAS*, **498**, 2391
- Olivares, V., Salome, P., Combes, F., et al. 2019, *A&A*, **631**, A22
- Pandya, V., Fielding, D. B., Bryan, G. L., et al. 2022, *arXiv e-prints*, [arXiv:2211.09755](https://arxiv.org/abs/2211.09755)
- Pasha, I., Mandelker, N., van den Bosch, F. C., Springel, V., & van de Voort, F. 2022, *MNRAS*
- Peng, Y., Maiolino, R., & Cochrane, R. 2015, *Nature*, **521**, 192
- Peng, Y.-j., Lilly, S. J., Renzini, A., & Carollo, M. 2012, *ApJ*, **757**, 4
- Peng, Y.-j., Lilly, S. J., Kovač, K., et al. 2010, *ApJ*, **721**, 193
- Pichon, C., Pogosyan, D., Kimm, T., et al. 2011, *MNRAS*, **418**, 2493
- Pillepich, A., Springel, V., Nelson, D., et al. 2018, *MNRAS*, **473**, 4077
- Planck Collaboration, Ade, P. A. R., Aghanim, N., et al. 2016, *A&A*, **594**, A13
- Roediger, E., Bruggen, M., Owers, M. S., Ebeling, H., & Sun, M. 2014, *MNRAS*, **443**, L114
- Schaap, W. E., & van de Weygaert, R. 2000, *A&A*, **363**, L29
- Schawinski, K., Urry, C. M., Simmons, B. D., et al. 2014, *MNRAS*, **440**, 889

- Schaye, J., Crain, R. A., Bower, R. G., et al. 2015, *MNRAS*, **446**, 521
- Simha, S., Burchett, J. N., Prochaska, J. X., et al. 2020, *ApJ*, **901**, 134
- Singh, A., Mahajan, S., & Bagla, J. S. 2020, *MNRAS*, **497**, 2265
- Song, H., Laigle, C., Hwang, H. S., et al. 2021, *MNRAS*, **501**, 4635
- Sousbie, T. 2011, *MNRAS*, **414**, 350
- Sousbie, T., Pichon, C., & Kawahara, H. 2011, *MNRAS*, **414**, 384
- Springel, V. 2010, *MNRAS*, **401**, 791
- Springel, V., White, S. D. M., Tormen, G., & Kauffmann, G. 2001, *MNRAS*, **328**, 726
- Springel, V., White, S. D. M., Jenkins, A., et al. 2005, *Nature*, **435**, 629
- Strauss, M. A., Weinberg, D. H., Lupton, R. H., et al. 2002, *AJ*, **124**, 1810–1824
- Terrazas, B. A., Bell, E. F., Pillepich, A., et al. 2020, *MNRAS*, **493**, 1888
- Trussler, J., Maiolino, R., Maraston, C., et al. 2020, *MNRAS*, **491**, 5406
- Vulcani, B., Poggianti, B. M., Moretti, A., et al. 2019, *MNRAS*, **487**, 2278
- Walters, D., Woo, J., & Ellison, S. L. 2022, *MNRAS*, **511**, 6126
- Wang, Y., Zhai, Z., Alavi, A., et al. 2022, *ApJ*, **928**, 1
- Welker, C., Bland-Hawthorn, J., van de Sande, J., et al. 2020, *MNRAS*, **491**, 2864
- Wilde, M. C., Elek, O., Burchett, J. N., et al. 2023, *arXiv e-prints*, [arXiv:2301.02719](https://arxiv.org/abs/2301.02719)
- Williams, R. J., Quadri, R. F., Franx, M., van Dokkum, P., & Labbé, I. 2009, *ApJ*, **691**, 1879
- Winkel, N., Pasquali, A., Kraljic, K., et al. 2021, *MNRAS*, **505**, 4920
- Xu, W., Guo, Q., Zheng, H., et al. 2020, *MNRAS*, **498**, 1839
- Zheng, H., Liao, S., Hu, J., et al. 2022, *MNRAS*, **514**, 2488
- Zinger, E., Dekel, A., Kravtsov, A. V., & Nagai, D. 2018, *MNRAS*, **475**, 3654
- Zinger, E., Pillepich, A., Nelson, D., et al. 2020, *MNRAS*, **499**, 768